

Peter A. Bandettini, Ph.D.

Characterizing and Utilizing fMRI Fluctuations, Patterns, and Dynamics

Section on Functional Imaging Methods, Laboratory of Brain and Cognition, NIMH

Section 1: Overview.....	2
Section 2: Research Themes.....	4
Theme 1: Spontaneous Fluctuations.....	4
1A. Introduction: Removing the noise and exploring the signal.....	4
1B. Progress report.....	4
1B-1. Impact of global signal regression on resting state data.....	4
1B-2. Multi-echo acquisition to sort ICA components and to minimize motion effects.....	5
1B-3. Periodic changes in correlation.....	7
1C. Current and Future Experiments	8
1C-1. Spatial heterogeneity of between-hemisphere motor strip correlation.....	8
1C-2. Clustering of resting state correlations.....	9
1C-3. Characterization of dynamic behavior of resting state networks.....	10
1C-4. Detection of mental states based on connectivity patterns.....	11
Theme 2: Activation Dynamics, Patterns, and Mechanisms.....	12
2A. Introduction: Pushing the limits of what we can extract from hemodynamics.....	12
2B. Progress report.....	13
2B-1: Finding activation in almost the entire brain with relatively simple tasks.....	13
2B-2. Representational similarity analysis.....	15
2B-3: Flip angle selection for fMRI revisited.....	16
2C. Current and Future Experiments.....	17
2C-1. Decoding of sub-voxel and TR timing differences.....	18
2C-2. Decoding “yes” and “no”	18
Theme 3: Anatomic MRI, perfusion, and fMRI calibration.....	19
3A. Introduction: Expanding the utility of fMRI and MRI.....	19
3B. Progress report.....	20
3B-1: Structural MRI changes with learning and exercise.....	20
3B-2: Robust pseudo-continuous arterial spin labeling at 7T.....	21
3C. Current and Future Experiments.....	22
3C-1: Valsalva vs. breath-holding effects effects.....	22
References.....	23
List of SFIM Publications since last BSC report.....	25
Section 3: Resources Requested.....	29

Section 1: Overview

The goal of the Section on Functional Imaging Methods (SFIM) is to better understand and more efficiently extract neuronally and, ultimately, clinically-relevant signal from MR images and fMRI time series. Most of our work since 2007 reflects this goal, as signal interpretation research and processing method development have constituted the bulk of the 47 papers and 89 abstracts produced by SFIM during this time period.

When the Unit (now Section) on Functional Imaging Methods (SFIM) was established in March of 1999, we had four ongoing themes (or projects): Technology, Methods, Signal Interpretation, and Applications. Over time, these categories have become less accurate in describing our primary research focus which had shifted more to MRI signal interpretation and methodology. Specifically, since 2007, we have been working towards obtaining a deeper understanding of the resting state and activation-based signal change characteristics, and designing better methods to extract neuronal information from noise and irrelevant signal. For this reason, we have organized our report into three themes: 1. Spontaneous fluctuations; 2. Activation dynamics, patterns, and mechanisms; and 3. Anatomic MRI, perfusion, and fMRI calibration.

Theme 1: Since 2007, the field of “resting state fMRI,” (rs-fMRI), also known as the study of “spontaneous fluctuations,” and a cornerstone of the field of “functional connectivity,” has exploded. Figure 1 shows the number of papers published in this area vs. year. Just under 800 papers are projected to be published on rs-fMRI in 2012 - about a third of all projected fMRI papers for this year.

This explosive rs-fMRI growth has resulted from a convergence of the availability of high MRI scanner stability and sophisticated processing methods, as well as a growing number of repeatable and relevant findings. Nevertheless, fundamental questions related to the scanning and processing methodology, neuronal and behavioral correlates, as well as the variability of rs-fMRI remain. In addition, complete and objective elimination of nuisance fluctuations remains an elusive goal. Our group is uniquely positioned to address these methodological and interpretive issues. We have focused much of our effort towards improving not only how resting state data can be acquired and processed but how it can be interpreted. We are also exploring what further information can be extracted and used. We plan to continue with this rich line of research – pursuing a deeper understanding of how correlated networks change across time scales as well as how networks can be classified and related to populations and to specific characteristics of individuals.

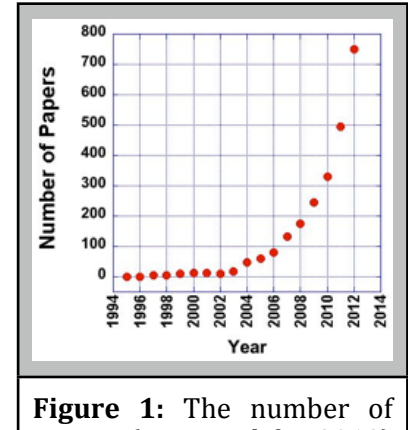


Figure 1: The number of papers (projected for 2012) per year that involve resting state fluctuations, showing an explosive growth.

We have data demonstrating a combined multi-echo pulse sequence and ICA-based processing stream for robust and automatic identification of relevant ICA components and for reduction of non-blood oxygenation level dependent (BOLD) fluctuations. From this foundation, we have developed a rs-fMRI based clustering of the entire brain into functional segments, as well as a method to minimize ubiquitous motion-related confounds in resting state data. We have also characterized, using a sliding window, the temporal variability of rs-fMRI correlation data. Lastly, we are developing methods for classifying time-varying mental states as a function of network correlation structure.

Theme 2: A cornerstone of SFIM research is the improved understanding and use of characteristics of the task-activated hemodynamic response. For over thirteen years, we have been probing the dynamics, spatial patterns, behavioral correlation, and variability of this response. Perhaps our most exciting and novel finding in this theme has been the discovery that even with a simple task, the entire brain shows evoked regionally-specific and uniquely shaped hemodynamic responses[1]. To obtain these results we averaged responses over nine hours from individual subjects performing a simple discrimination tasks, then processed the data with no assumptions about hemodynamic shape. Clustering of the responses showed clear responses throughout the brain. Also within this theme, we demonstrate that reduction of the MRI flip angle - having several advantages over a higher flip angle - does not result in a reduction in temporal signal to noise if physiologic noise dominates[2].

We also report here on our ongoing efforts towards better understanding the underlying mechanisms behind and limits of multivariate analysis – considering each voxel as part of a pattern of activity across relevant regions of the brain. Using a multivariate classification approach, we have been able to infer sub-TR (100 ms) and sub-voxel (ocular dominance column) relative activation sequences, and have been able to decode “yes” and “no” answers in subjects - both of these at about 90% accuracy.

Theme 3: Our group also values the importance of developing methods that are complementary to rs-fMRI and fMRI. A new area of research has emerged that is based on the measurement of anatomic MRI changes in individuals over short periods of time. We have established a processing pipeline for assessing changes in anatomy with exercise and learning[3, 4]. We continue to develop perfusion imaging methods, working closely with fMRI core facility. We have also developed an a high resolution, off-resonance corrected arterial spin labeling (ASL) approach at 7T resulting in perhaps the highest fidelity ASL-based perfusion images yet produced[5]. Regarding hemodynamic calibration, we show the utility of using the Valsalva maneuver. This finding may lead to implementation of a more simple and repeatable global calibration stress than that of hypercapnia.

Since 2007 our group has also produced a body of work that has involved a wide range of applications of cutting edge methods, but due to space limitations, this research will not be described. These topics include anatomic differences with autism[6], non-neuronal related release from adaptation[7], single stimuli activation profiles[8], movement-related theta rhythm assessment[9], unconditioned responses and implicit memory[10, 11], effects of task-correlated breathing[12], group differences in connectivity[13], verbal fluency[14], and regions differentially associated with task difficulty and decision making[15]. In the future, we plan to move more aggressively towards development of *individual* assessment methods. We believe that for fMRI to become more relevant to the mission of NIMH, it has to aid in assessing psychiatric and neurologic disorders on an individual basis – in much the same way that anatomic MRI is effective in identifying and monitoring an individual’s anatomic brain pathology. We are well-positioned to take this goal on, as we are working at 7T with novel pulse sequences and processing strategies.

This report is organized as follows: The themes are numbered 1 through 3. Within each theme, there are three sub headings: **A** is a brief introduction; **B** is the progress report which describes projects that have been completed after December of 2007 – most having resulted in published manuscripts; and **C** describes ongoing, unpublished projects. At the end of each project description, the section members and collaborators are listed in parentheses in alphabetical order, with the primary investigator in bold print. Collaborators from the fMRI core facility or elsewhere are in red.

Section 2: Research Themes

Theme 1: Spontaneous Fluctuations

1A. Introduction: An abundance of information and a proliferation of methods

As mentioned in the overview, a major focus of SFIM has been the better understanding of resting state fluctuations and the development of methods to more effectively separate neuronally-relevant fluctuations from artifactual fluctuations. In several areas, our work has had an impact on the field. Specifically, we have shown that global signal regression causes artifactual negative correlations in major networks[16], introduced a novel multi-echo technique that enables objective and clean selection of ICA components[17], and uncovered a unique periodic relationship between network fluctuations[18]. This theme contains a relatively large proportion of ongoing, unpublished work: Specifically we demonstrate preliminary results using seed voxel analysis to clarify cross-hemisphere motor connectivity in single subjects; introduce an effective resting state-based brain parcellation method that stems from our multi-echo based independent component analysis (me-ICA) approach; characterize, in detail, the dynamics of resting state networks, identifying the most and least stable pairwise network connections; introduce a promising method for characterizing cognitive states using resting state data, and lastly; propose an effective solution, also using me-ICA, to recently highlighted motion-related problems in resting state data interpretation.

1B. Progress report

1B-1. Impact of Global Signal Regression on resting state data.

The basis of rs-fMRI is the identification and characterization of the MRI fluctuations that relate to spontaneous and correlated neuronal activity. A major challenge is that many non-neural signals cause correlated fluctuations in fMRI time series. These artifactual signals include breathing and cardiac-related signal changes, head movement, and MRI scanner noise. One method to reduce these nuisance signals has been to average the signal over the entire brain - the global signal - for each time point, and regress this averaged time series out of the data. The assumption is that neural activity does not synchronously happen everywhere in the brain at the same time. Therefore, it follows that any fluctuations in the global signal can be removed, as they do not represent neuronal activity. While global signal removal does reduce temporal fluctuations, we demonstrate, as shown in Figure 2, that it introduces artifactual anti-correlated networks [16]. Several papers that have had global signal regression as a processing step have often showed strong anti-correlated networks of brain regions[19]. We demonstrate both theoretically and experimentally in our paper that global signal regression artificially creates negative or “anti-correlated” resting state signals. Our manuscript has had a high impact on the field. It has also elevated the discussion in the fMRI community of which

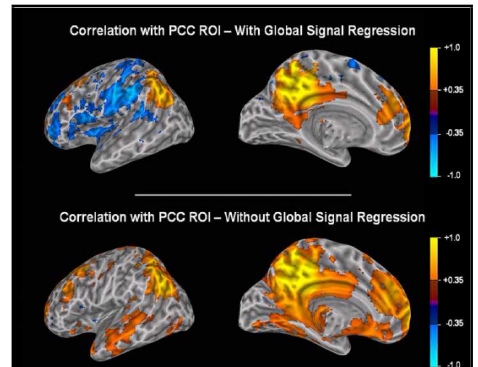


Figure 2: Correlation to a seed region in PCC are shown with and without global signal regression. The default mode network is visible both with and without global signal regression, but a negatively correlated network is only visible after the regression.

processing steps introduce or eliminate artifacts with minimal signal corruption. (*P. A. Bandettini, R. M. Birn, D. A. Handwerker, T. B. Jones, K. Murphy*)

1B-2. Multi-echo acquisition to sort ICA components and to minimize motion effects

An ongoing challenge has been to remove the large fraction of non-neuronal fluctuations from rs-fMRI time series. Work on characterizing and removing non-neuronal fluctuations has focused on time series modeling based on external measures of physiologic processes. In this study, we fully embrace and carry forward the proposed work in our last BSC report from 2007 on using TE-dependence to separate BOLD from non-BOLD time signal so that non-BOLD - thus non-neuronally relevant - fluctuations can be removed. BOLD signal changes are manifest as changes in T_2^* , which can be characterized as showing a linear increase in fractional signal change with echo time (TE). Motion, system instabilities, and inflow effects can be manifest as changes in longitudinal relaxation, T_1 or proton density, S_0 but not typically T_2^* .

Here we show the utility of collecting multi-echo EPI (me-EPI) to clearly separate BOLD signal fluctuations from non-BOLD signal fluctuations. We collect three-echo me-EPI data and then apply independent component analysis (ICA) on the echo-concatenated time series data resulting in each ICA map consisting of three images, each collected at a different TE. On a voxel-wise basis, the change of the component's percent signal change with TE is fit separately to ΔR_2^* and ΔS_0 signal change models, and the fit quality is computed as an F-statistic. Each component is characterized by two metrics, κ for its BOLD likeness and ρ for its non-BOLD likeness. Figure 3 shows that resting state BOLD components and non-BOLD noise components are differentiable according to these metrics.

When the κ values of all of the ICA components are sorted and plotted as a spectrum, high κ and low κ value regimes are clearly evident, separated by a boundary (an elbow in the curve). When the ρ values corresponding to κ values are given, it is clear that the majority of components have high κ and low ρ , or vice-versa, thus distinguishing BOLD and non-BOLD components. The differentiation of BOLD and non-BOLD components not only enables sorting of ICA components for subsequent clustering analysis (shown in IC-2) but also allows for the use of low κ component time series for de-noising in task-based fMRI or seed based rs-MRI.

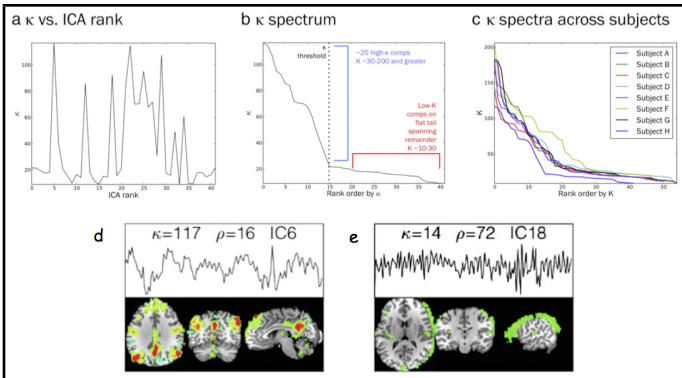


Figure 3: For a representative subject, κ score vs (a) ICA rank (variance explained), and (b) rank by κ (κ spectrum). The κ spectrum, is an L-curve with two distinct regimes: high κ ($\kappa > 20$) and low κ ($\kappa \leq 20$), with low κ components on a linear tail. (c) κ spectra for 8 subjects. (d) Example of high κ and low κ component maps. Each panel shows the time course and thresholded ΔR_2^* map. Components are annotated with κ -score, ρ -score, and ICA component number.

We demonstrate in our manuscript introducing this approach[17], that de-noising performed by removing the regressors identified as those with low κ components is more effective than standard methods involving modeling and regressing out the noise - particularly in problematic regions such as hippocampus, thalamus, and brainstem.

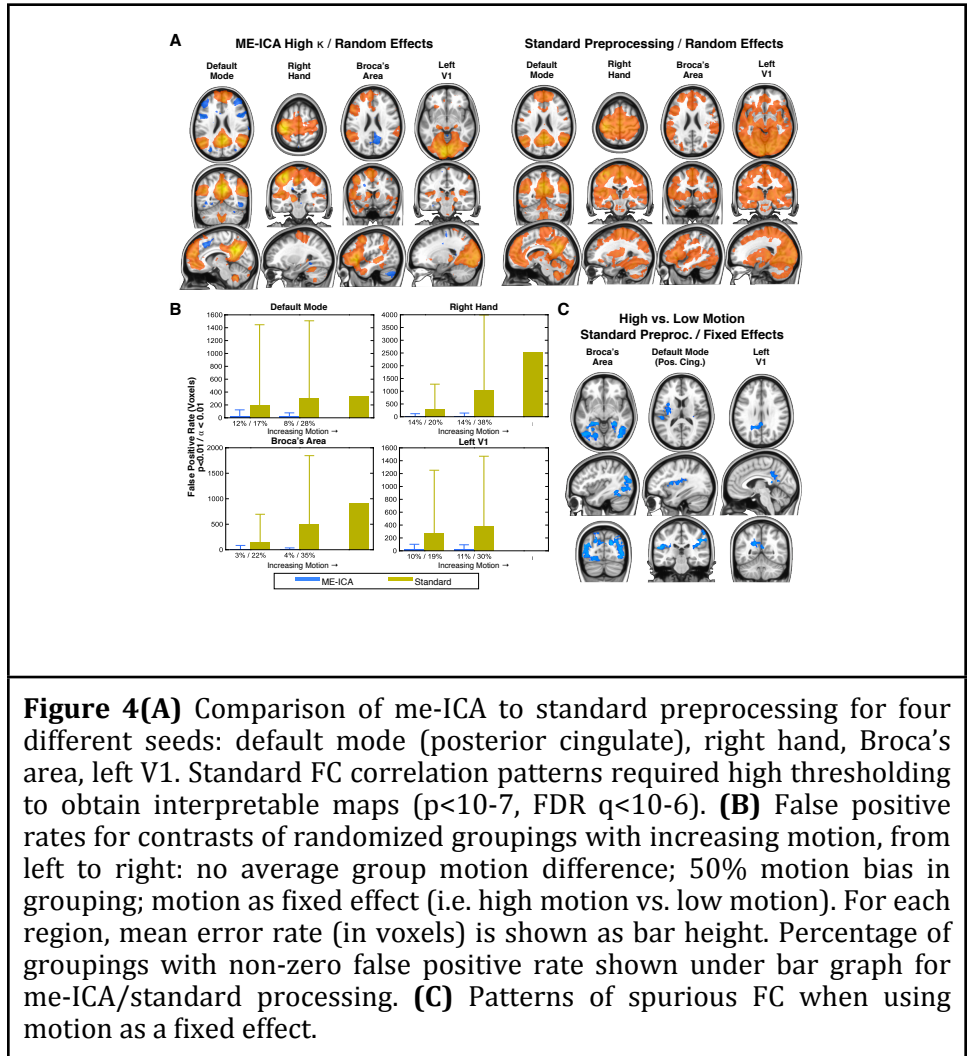
It has recently been shown that in-scanner

subject head motion leads to systematic patterns of false positives in population-level rs-fMRI analysis[20]. This artifact is worst for group contrasts of cohorts with different levels of in-scanner motion (i.e. adult vs. child, healthy vs. pathological), and is a potential roadblock to further resting state fMRI - based research.

Here we show that me-ICA enables a principled and robust approach to minimizing the problem of spurious functional connectivity (FC) patterns caused by motion and other artifacts. After decomposing multi-echo data with ICA and separating BOLD from non-BOLD components based on echo-time (TE) dependence, the BOLD-based ICA components are used to compute FC. We then focus exclusively on the BOLD ICA components. Computing an individual-subject me-ICA functional connectivity map for a region of interest (ROI) involves *computing the correlation of its ICA series with the ICA component series of all other voxels*. In contrast, the typical approach to computing FC maps involves motion regression, band pass filtering, and then Pearson correlation.

The me-ICA seed-based FC approach was compared to standard seed-based FC approach at the population level. Thirty-three subjects were scanned for 10 minutes EPI during rest (Siemens 3T Tim Trio, 32-channel). Figure 4 A shows analyses for the full cohort. Figure 4 B is a comparison of me-ICA and standard processing. For all ROIs, me-ICA FC group contrasts are populated in only 10% of all random and biased groupings, and with small error rates, if any (20 voxels on average).

No increase in me-ICA FC false positive rate is found as groupings are increasingly biased according to motion. In contrast, standard FC group contrasts have increased false positive rates as groupings are biased by motion. We conclude that me-ICA FC is a principled and straightforward solution to the problem of spurious FC due to motion artifact. (*P. A. Bandettini, E. Bullmore, N. Brenowitz, J. W. Evans, S. J. Inati, P. Kundu, W.-M. Luh, V. Roopchansingh, Z. S. Saad*)



1B-3. Periodic changes in correlation.

In most rs-fMRI studies, data are collected for 5-10 minutes and analyzed across the entire scan duration to create connectivity maps with high reproducibility. However, when observed over shorter windows of time, correlation strengths between regions show temporal variations. In this study[18], we show that these changes in correlation strength appear to vary in a periodic manner.

Figure 5 shows this variation in correlation for two slices in the brain. Figure 5A shows the posterior cingulate cortex (PCC) region used for the seed time course. Figure 5B shows the correlation map obtained using that seed over the entire ten minute time course. Figure 5C shows the changes in the correlation with the seed voxel in 32 sec windows. Figure 5D shows the time course of the seed and another region in the motor cortex (not typically correlated with anterior cingulate). Figure 5E shows the correlation values between the seed and the motor cortex over time, showing an average of about zero yet semi-periodic changes across a wide range of positive and negative correlation values.

By calculating the power spectrum of these correlation time series, we show that the correlation fluctuations appear to have several distinct frequency peaks. While all correlations are to a single PCC seed, the peak correlation change frequency varies by brain region. Figure 5F shows relative power spectrum magnitude maps at four frequencies. The red regions for each column of slices in a volume are the peak frequency magnitudes corresponding to the sliding window correlation change power spectrum below.

While we cannot fully explain this periodicity, we should note that this does not imply that networks are necessarily “communicating” with each other. Rather, this appears to be a “beat frequency” effect that might prove useful in probing the most relevant of network fluctuation frequencies. Also, this approach might open up a methodology for probing differences in frequency content between regions.
(P.A. Bandettini, J. Gonzalez-Castillo, D. A. Handwerker, V. Roopchansingh)

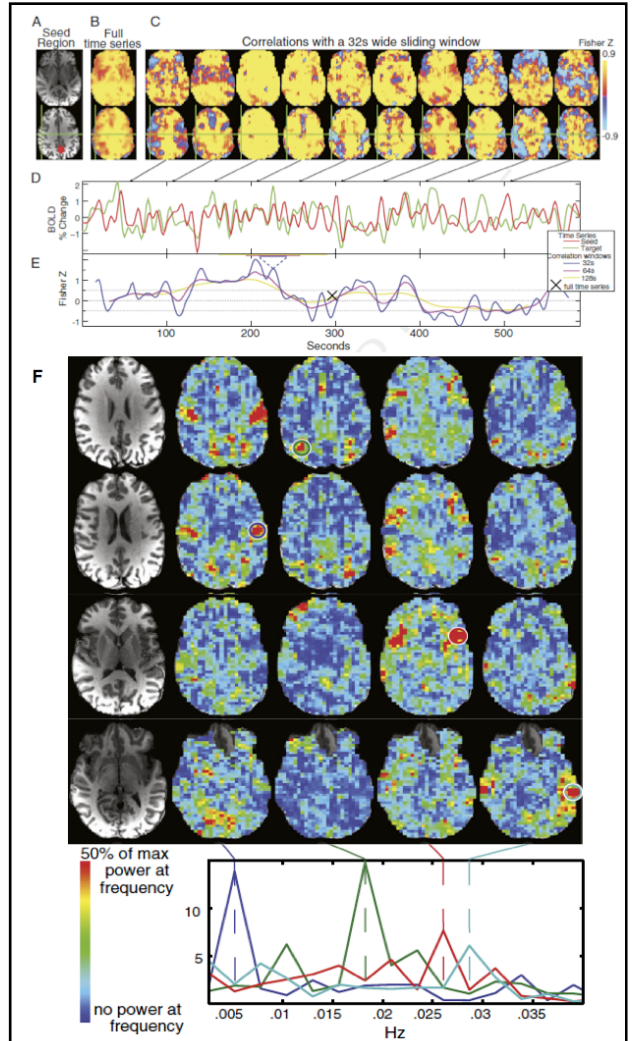


Figure 5: **(A)** Posterior cingulate (PCC) seed region (red highlight) that was used. **(B)** Correlation map created from the seed using the entire ten minute time series. **(C)** Correlation maps created over 32 s temporal windows centered at the time points in the connected figures D and E. **(D)** Sample time series from the seed region (red) and a voxel at the green crosshairs (motor cortex region). **(E)** Correlation values over time for the sample time series show that the temporal correlation varies over time but has minimal dependence on correlation window. **(F)** Power spectrum of correlation changes with PCC. Maps in each column correspond to frequency peaks.

1C. Current and Future Experiments

1C-1: Spatial heterogeneity of between-hemisphere motor cortex correlation

Analysis of correlated rs-fMRI signals have revealed detailed patterns of functional organization. Studies taking advantage of the increased SNR using 7T MRI scanners have been able to discriminate functional networks at increasingly fine scales along cortical folds and layers. In this preliminary study, seed-based correlation maps using ROIs along the sensorimotor strip are tracked in order to assess detailed, localized variations in motor strip connectivity. A goal of this study is to determine if regionally specific connectivity differences, as revealed through rs-fMRI of single subjects exists between left and right motor regions. Using an EPI sequence at 7T with a 32-channel phased array coil, four 10-minute rest runs and four 5-minute task activation block runs where subjects were instructed to move, during separate blocks, their tongue, fingers, eyebrows, or toes in 16 sec intervals were acquired (TR=2; 2mm isotropic; 96x96x54 grid). Runs were aligned and mapped to the surface with seed regions ($\sim 0.4 \text{ cm}^3$) drawn along the motor cortex of the each hemisphere using the block results from the task runs within sulcal parcellations as landmarks. The principal singular vectors of the resting-state run time series within the drawn ROIs were used as seeds for correlation maps to the rest of the brain. Series of correlation maps along both hemispheres for each resting state run were rendered on the surface map to track changes in correlation with changes in seed regions.

Seed-based correlation analysis of resting state data revealed strongly localized, bilaterally symmetric correlations along the entire sensorimotor strip, yet showed substantially reduced correlations in areas corresponding to the hand in agreement with non human primate results using anatomic tracers[21]. These results suggest that, in spite of regional differences in factors such as baseline noise level and blood volume, the resting state correlation between time series across regions appears to be

a sensitive measure of the “degree” of connectivity between areas. This finding reveals that resting state correlation analysis in a single subject yields previously unknown, yet literature-supported, functional organization and degree of connectivity in the human sensory-motor area.

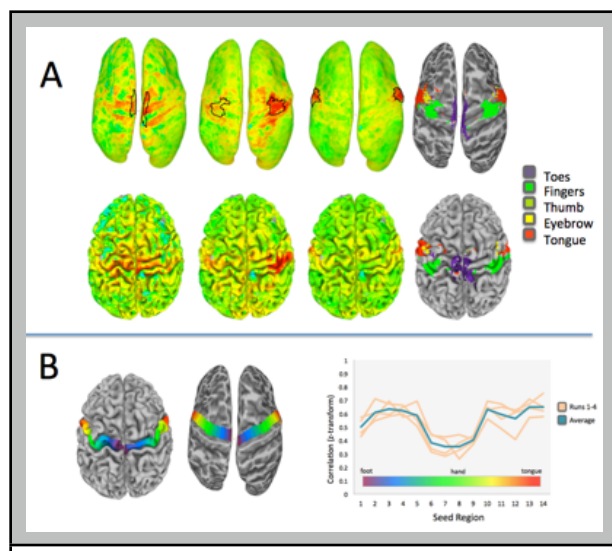


Figure 6: (A) Cross-hemisphere resting state correlations and areas of activation with specific movements in flattened and non-flattened display. (B) Color coded motor strip locations and corresponding cross-hemisphere resting correlation magnitude.

We plan to continue this seed voxel exploratory approach to assess spatial variations in correlations across a wide range of brain networks. Specifically, we will explore other networks that are known to have varying colossal connections to determine how widely applicable this observation is. We will also attempt to use this precise seed voxel tracing approach to probe functionally related regions that have colossal connections versus those that don't. Lastly, we will perform diffusion tensor imaging-based tract tracing with tract seed points determined from the spatially variant connectivity maps as an approach to integrate and validate DTI and rs-fMRI information. (P. Bandettini, P. Guillod, S. J. Inati, P. Kundu)

1C-2: Clustering of resting state correlations

A major goal in rs-fMRI is the whole-brain mapping of functional cortical networks down to the scale of voxels from a single dataset. Promising results have been obtained on highly subject-averaged data, however, our ultimate goal is to use the characteristics of these networks as individual biomarkers. Towards this goal, we have developed an approach, based on our me-ICA method (from 1B-2) that converges on stable and consistent areas with very few averages. The maps that we produce can also predict subject-specific activation patterns associated with activation-based paradigms.

Seven subjects were scanned with 10 min rest runs and with several task-activation runs consisting of the following paradigms: face vs. objects differentiation, sense vs. nonsense sentence differentiation, tongue vs. toe movement. Imaging was performed on a General Electric (GE) 3 Tesla GE Signa HDx MRI scanner with a GE 8-channel receive-only head coil. Anatomical images were acquired using a T1-weighted MPRAGE sequence. Functional images were acquired with a *multi-echo EPI* sequence (TR 2.5 s, flip angle 90°, matrix size 64x64, in-plane resolution 3.75 mm, FOV 240 mm, 31 axial slices, slice thickness 4.2 mm with 0.3mm gap, acceleration factor 2). Three echoes were acquired with the shortest possible echo times, TE = 15ms, 39ms, and 63ms. Multi-echo data were analyzed with me-ICA to reveal BOLD ICA components and remove non-BOLD ICA components. This non-BOLD component removal is fundamentally important in the success of these results as the clustering method was based on the voxel-wise grouping and differentiation based on its unique belonging “signature” to each ICA component.

This exquisitely detailed hierarchical structure is shown in Figure 7. Large modules (from low level clustering, i.e. k=10 clusters) reflect classical neuroanatomy. These modules correspond to regions such as superior, middle, and inferior frontal and temporal gyri; premotor, motor, sensory, and insular cortices; cingulate and visual areas, etc. Smaller modules (from high level clustering, i.e. k=350 clusters) reflect functionally specific areas. These modules correspond to regions in the motor cortex such as lateralized hand, foot areas, as well as language areas (Broca’s and Wernicke’s), visual areas (V1/V2), and many others. The novel implementation of hierarchical clustering

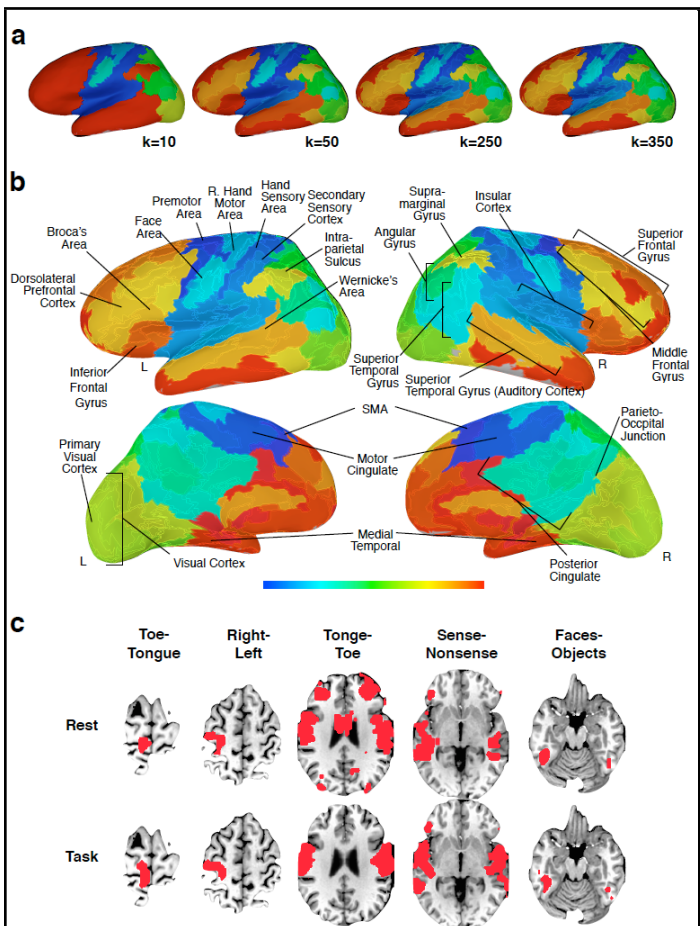


Figure 7: (A) Functional organization ($n=7$) at increasingly high levels of clustering. Lower cluster levels show large modules. Higher cluster levels show increasing differentiation of functional areas within color ranges determined by lower level clustering. (B) Labeled map of the $k=350$ functional organization. (C) Comparison of task activated regions and resting state clusters in a single subject, showing a close correspondence.

approach carried the organization of low level clustering to high level clustering in terms of cluster index ranges. This means that color proximity (i.e. on a color bar) of cortical areas indicates functional relatedness, and color separation indicates functional distinctness. This coloring scheme greatly aids in interpretation of high level clustering, especially in mapping major functional boundaries.

It was found that cluster maps converged as the number of subjects used in group analysis was increased. A stable organization was achieved using only 7 subjects. This indicates a large increase in statistical power of this method over prior methods that do not use me-ICA, ICA-based clustering, and cortical surface-based averaging. Since analysis was conducted on the cortical surface, the rapid convergence also suggests strong conservation of functional organization on the cortical sheet.

This novel implementation of hierarchical clustering was able to create a community structure of brain organization, showing how large modules at low levels of clustering are related to smaller modules at high levels of clustering. We found that the 30-50 BOLD components from individual subject high dimensional me-ICA have localization to specific, finely delineated functional areas. The ability to consistently identify functional areas without functional localization tasks could also be of value as a biomarker for individual differences or disorder characterization. (*P. A. Bandettini, N. Brenowitz, J. Evans, P. Guillod, S. J. Inati, P. Kundu, W.-M. Luh*)

1C-3: Characterization of dynamic behavior of resting state networks

An assumption has been that connectivity patterns are stable for the duration of the scan. The purpose of this work is to carry forward our work in 1B-3 and characterize the temporal variation of resting state connectivity within a continuous 1 hour resting state scan. From this we are able to determine the most and least stable networks. We first characterize connectivity matrix variability as a function of scan duration and then map the most and least stable pairwise connections.

After segmenting the brain into 100 functional units for use in connectivity matrix creation, we compared pairs of matrices that were created by averaging the signal over varying amounts of time ranging from 2 to 30 minutes. Figure 8 shows the correlation between each of the pairs of matrices. The correlations begin to show decreasing similarity below 10 minutes, and continue to drop sharply down to 2 minutes.

To further dissect the variability of the

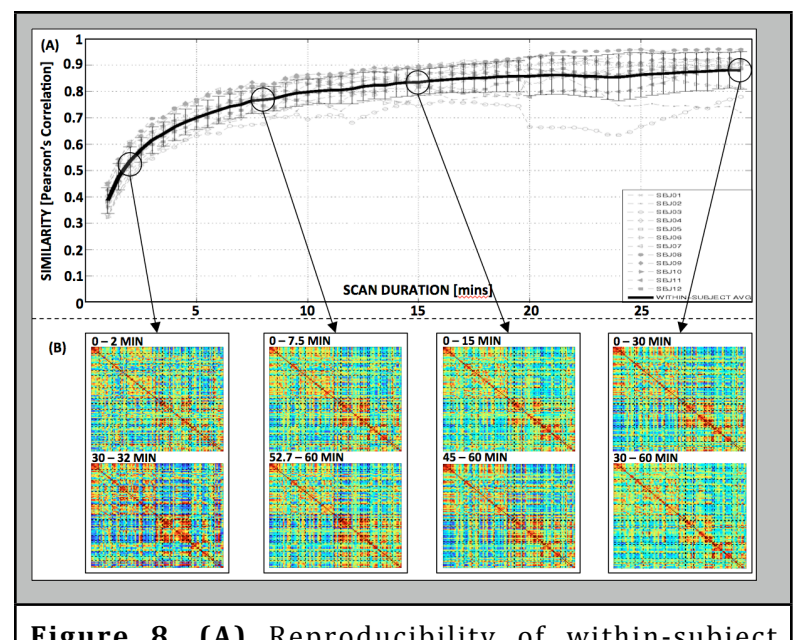
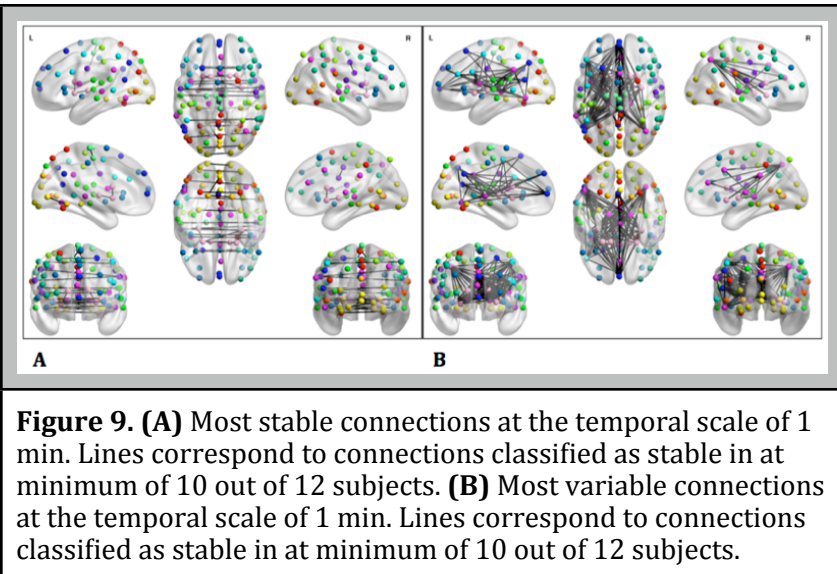


Figure 8. (A) Reproducibility of within-subject connectivity patterns as a function of scan duration. **(B)** Representative connectivity matrices for durations of 2min, 7.5min, 15min and 30min. It can be observed that connectivity patterns become more similar as scan duration increases. For durations below 5 minutes, reproducibility decreases.



cortical connections, we used a sliding window correlation analysis with a window duration of 1 min and a window step of 1 s. We then sorted the pairwise connections from most to least variable. While some connections remain quite stable across time, others seem to vary considerably. Figure 9 A shows most stable connections across all subjects. It can be observed that stable connections tend to be interhemispheric and symmetric. Figure 9 B shows connections that vary the most across time in all subjects. The pairwise connectivity patterns in this case are quite different, appearing to

correspond to these between subcortical regions and high order cognitive regions in frontal and predominantly left parietal cortex.

These network variability maps provide a unique insight into the dynamic brain activity during resting state. We will continue to explore these across timescales and begin to explore subject-wise and behavioral correlates as they may reveal insights into principles of dynamic brain organization.
(P. A. Bandettini, C. Chang, J. Gonzalez-Castillo, D. Handwerker, S. J. Inati, M. Robinson, V. Roopchansingh, Z. S. Saad, Z. Yang)

1C-4: Detection of mental states based on connectivity patterns.

An approach to understanding the biological significance of dynamic changes in connectivity patterns is to investigate whether they correlate with explicit behavior. If observed changes in functional connectivity reflect changes in the functional organization of the brain as it switches from one task or mental state to another; then whole-brain functional connectivity patterns should allow us to ultimately classify a subject's cognitive state or task being performed. To begin to evaluate this possibility, we ask subjects to engage in different tasks (2-back, simple math, watching a video, and rest) while being continuously scanned.

A 60 s sliding window, with step length of 1 sec was used. Correlation analysis obtained snapshots of connectivity across the whole brain as scanning progressed. For each sliding window, the upper half of the connectivity matrix was transformed into a vector. Vectors were concatenated horizontally to produce a new matrix (#windows x #Connections) that contained information about the evolution of connectivity patterns as shown in Figure 10. Because of the high dimensionality of this matrix (each window has 4950 connectivity values), it is very difficult to evaluate if different tasks are associated with different patterns of connectivity. For identification and visualization, we used multidimensional scaling (MDS) to reduce the dimensionality to a 3D space.

In Figure 11 each window is represented as a dot in a 3D space. Sliding windows that contain transitions between tasks have been removed. Remaining points, after removal of transitions, have

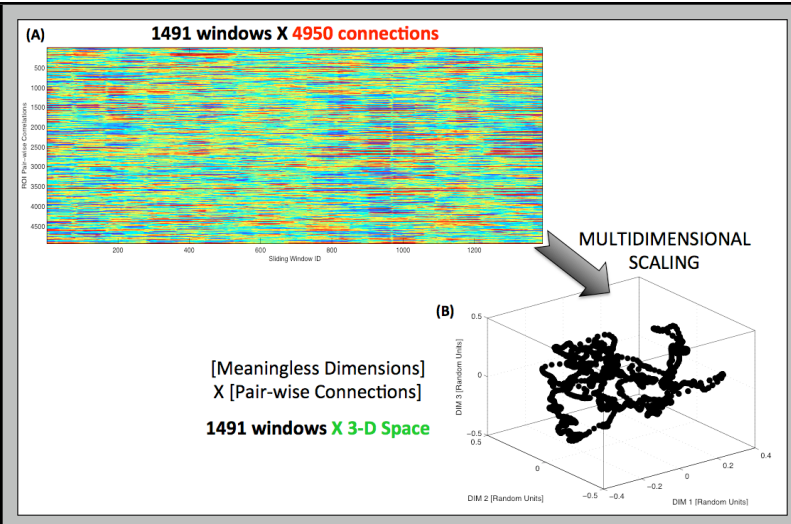


Figure 10. (A) Evolution of whole-brain connectivity as scanning progresses using sliding window analysis (win length=60s, win step=1s). A row in this matrix corresponds to the temporal evolution of the connectivity values for a given pair-wise connection. A column in this matrix corresponds to the overall connectivity pattern of the brain in a given window of time. (B) Result of applying non-metric multidimensional scaling to the matrix on (A). After MDS, each window can be shown as a point in 3 dimensional space.

clear separation of tasks does not occur for all subjects. The use of more differentiable tasks, other dimensionality reduction techniques, or prior selection of most or least variable networks may help improve segregation of tasks based on connectivity profiles. (*P. A. Bandettini, C. Chang, J. Gonzalez-Castillo, D. Handwerker, S. J. Inati, M. Robinson, V. Roopchansingh, Z. S. Saad, Z. Yang*)

Theme 2: Activation Dynamics, Patterns, and Mechanisms

2A. Introduction: Pushing the limits of what we can extract with hemodynamics

After twenty years of investigation on the activation-related fMRI signal changes, it's encouraging that new information continues to be extracted as methods are developed and tested. Our group has made several contributions in this area since 2007. First, we have discovered that with sufficient amount of averaging and with a model-free approach, nearly the entire brain is uniquely activated by even simple tasks. This is perhaps our highest profile paper in the past few years. Next, we have pioneered a method, known as representational similarity analysis, to characterize fine scale patterns of activation that reside within blobs. These patterns are proving to be information-rich and complementary to the mapping large scale activations. With regard to our MRI-based work, we have demonstrated that, in typical studies where physiologic noise dominates, a wide range of non-Ernst angle flip angles can suffice without a loss in functional contrast to noise. Our current and future work primarily involves carrying forward fMRI "decoding" methods. Specifically, we have developed a

been colored according to the task the subject was performing during that period of time (gray = rest; cyan = 2-back task; green = math computation; yellow = video observation). The figure suggests that brain connectivity does change with task, and are stable during performance of the task. Unfortunately a

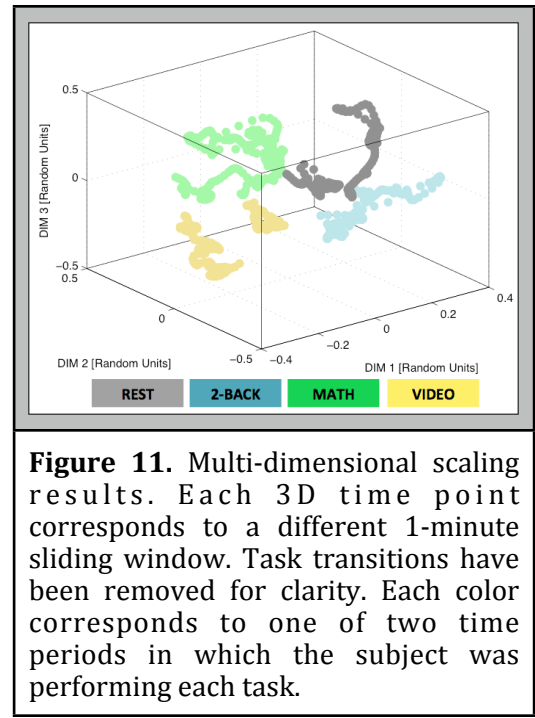


Figure 11. Multi-dimensional scaling results. Each 3D time point corresponds to a different 1-minute sliding window. Task transitions have been removed for clarity. Each color corresponds to one of two time periods in which the subject was performing each task.

method for differentiating with high accuracy, sub-voxel sub-TR onset times - differentiating 100ms onset differences between left and right ocular dominance column activation. Also, towards the goal of exploring the sensitivity limits of “decoding” approaches, we have developed a method for accurately differentiating simple “yes” and “no” cortical responses.

2B. Progress report

2B-1. Finding activation in almost the entire brain with relatively simple tasks

In the past, task-based functional MRI (fMRI) studies have supported a localizationist view of brain function, as typically, only a handful of regions have shown significant activation with a task or stimulus. Here, this view is challenged with evidence that under high contrast to noise conditions, fMRI activations extend well beyond areas of primary relationship to the task - *appearing in over 95% of the brain* for a simple visual stimulation/attention control task[1]. Moreover, we show that response shape varies across regions and can deviate substantially from a typical canonical response. Whole-brain parcellations based on those response shape differences produce distributed clusters that are anatomically and functionally meaningful, symmetrical across hemispheres, and reproducible across subjects. This result has the potential to fundamentally alter how we understand and model brain activation.

Three subjects were scanned on a General Electric 3T MRI scanner. All subjects underwent 100 functional runs, which consisted of five blocks of stimulation. Each block consisted of 20 s flickering checkerboard at 8 Hz + letter/number discrimination task and 40 s of rest. For the letter/number discrimination task, subjects responded using a response box with their right hand. Data were analyzed with AFNI (pre-preprocessing, and statistical analysis), and MATLAB (clustering).

We used three response models for activation: 1. A sustained response model (SUS) consisting of the convolution of a gamma-variate function with a boxcar function that follows the experimental paradigm; 2. An onset+sustained+offset model (OSO) that includes transitory responses at blocks onset/offsets in addition to the sustained response; and 3. An unconstrained model (UNC) consisting of 30 impulse functions spanning the duration of a single on/off cycle (60 s) and therefore setting no a priori constraints on response shape other than agreement with task periodicity.

We found that the extent of activations increased significantly with number of runs (Nrns) inputted to the analysis as well as with a relaxation of the predictive BOLD response shape constraints. Figure 12 shows how activation extent increased with increases in number of runs. For all subjects, significantly active voxels at Nrns = 100 represent on average over 71% of the imaged brain for the SUS model; and over 89% for the other two models at $P_{FDR} < 0.05$. Conversely, for Nrns = 5, which represents a typical

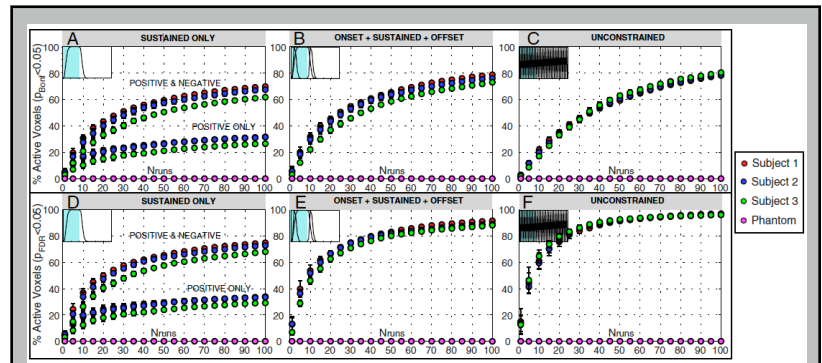
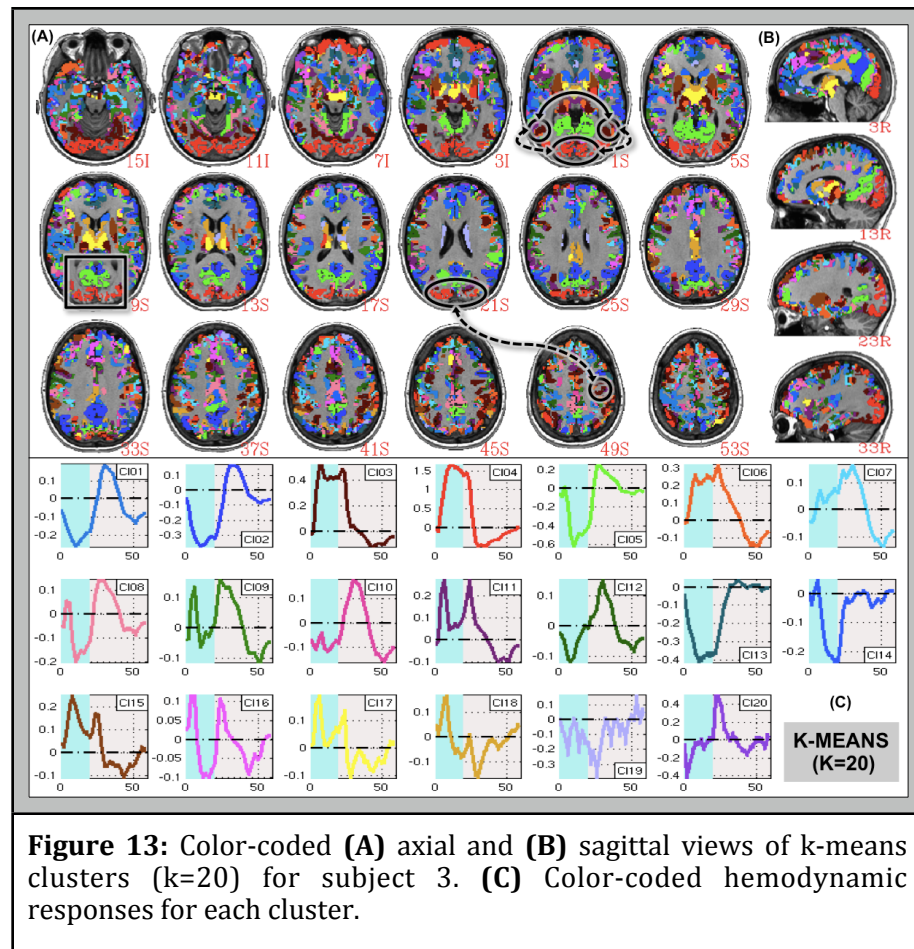


Figure 12: Activation extent results for the three response models. A-C show results for $P_{\text{bonf}} < 0.05$ and D-F for $P_{\text{FDR}} < 0.05$. The significantly active volume increased with number of runs in all subjects and models.

number of runs per condition in fMRI experimentation, activated voxels represented ~20% of the imaged volume at $\text{PFDR} < 0.05$ for the SUS analysis and between 35 and 44% for the other two analyses. Active voxels are defined as those where the model accounts for a significant amount of variability in the data (F-stat) at $\text{P}_{\text{FDR}} < 0.05$ or $\text{P}_{\text{Bonf}} < 0.05$. Within-subject averaging reduced random noise while keeping non-random signal levels unaffected. Statistically significant signal changes (sometimes less than 0.2%) time-locked with the task could be observed in almost every location of the brain when 100 runs were averaged. Response shape and magnitude varied significantly across regions. Some regions responded in a sustained positive manner for the whole duration of the task epochs (e.g., occipital, insular and left motor cortex), but others responded more prominently during task-switching periods (e.g., occipito-parietal junction). Several regions responded with negative deflections during active epochs (e.g., some parietal locations, right motor cortex). In regions that responded similarly (e.g., sustained), there were differences in onset, offset, and steady-state shape.

Parcellation of the whole brain activation data was accomplished as follows: Voxels with similar response profiles were spatially clustered using both k-means and hierarchical clustering on the voxel-wise BOLD responses calculated using all 100 runs per subject. Parcellations were computed only for cortical and subcortical gray-matter voxels, excluding the cerebellum. Figure 13 shows the k-means decomposition for a representative subject and $k=20$. The resulting topography is symmetrical across hemispheres, anatomically meaningful, and reproducible across subjects. Hemispheric symmetry is evident in the occipital cortex, superior temporal cortex, anterior insula, hippocampus, and in subcortical structures, such as the thalamus and the putamen.



Primary visual and primary hand motor cortices correspond to different clusters. The visual cortex is segmented into several regions both in the anterior-posterior (A-P) and medial-lateral (M-L) directions. For example, in the M-L direction V1 and V5 are segregated. In the A-P direction, V1 and higher visual processing areas closer to the parieto-occipital junction are also part of different clusters. In most cases, clusters did not appear in the form of a single contiguous agglomeration of voxels but as distributed sets of nodes. Grouping patterns go beyond hemispheric symmetry, and in some cases resemble

connectivity patterns similar to those present in resting-state data. For example, the area CL03 resembles a motor control network with nodes in the left primary motor hand cortex, medial supplementary motor cortex, and postero-lateral thalamus. Cluster CL02, with nodes in the bilateral infero-lateral parietal cortex, posterior cingulate, and ventro-medial frontal cortex, resembles the default-mode network. Figure 13 C shows cluster-averaged responses. All clusters display responses time-locked with the experimental paradigm.

These findings highlight the exquisite detail in fMRI signals beyond what is normally examined, and emphasize both the pervasiveness of false negatives, and how the sparseness of fMRI maps is not a result of localized brain function, but a consequence of high noise and overly strict predictive response models. It also shows how inter-regional variability in the hemodynamic response to tasks can be used to functionally parcellate the whole brain in a manner similar to resting-state scans. Differences in functional parcellations between task-state and resting-state may provide good markers for identification of clinical populations. We plan to continue this work at high field, using me-EPI, and with higher sensitivity RF coils in hope that we can achieve a temporal signal to noise such that the necessary scan duration to obtain these results is more realistic. We also plan to explore the reproducibility of these results with other tasks. (*P. A. Bandettini, N. Brenowitz, J. Gonzalez-Castillo, D. Handwerker, S. J. Inati, Z. S. Saad*)

2B-2. Representational similarity analysis

Monkey single-cell recordings have shown that primate inferotemporal (IT) neurons respond selectively to visual features occurring in natural images as parts of objects. Kiani et al.[22] have demonstrated that monkey-IT response patterns cluster according to natural categories. Human neuroimaging has demonstrated conventional-category information in human IT cortex in both focal activations and widely distributed response patterns. However, a focus on category-average responses has precluded addressing if a categorical structure is inherent to the representations and, if so, what the natural categories are.

This study[23] combines human and monkey data from hi-res fMRI and single-cell recordings, respectively. We investigate response patterns elicited by the same 92 photographs of isolated natural objects in IT cortex of both species. Each stimulus image forms an independent condition. No predefined stimulus grouping is implied in either the experimental design or the core analyses to be applied. Because response patterns are difficult align between species or even among human subjects, we relate monkey and human representations by considering, for each pair of stimuli, the similarity of the response patterns the two stimuli elicit. This approach also allows us to relate both species to computational models exposed to the same stimuli.

Monkeys performed a fixation task while presented with the images in rapid succession. Responses of more than 600 cells were recorded in two monkeys (right and left anterior IT cortex, respectively). Human subjects detected color changes occurring at fixation during image presentation while we measured response patterns with hires fMRI (3T, SENSE, voxels: 1.95x1.95x2mm³).

Figure 14 A shows that IT response patterns across these two species cluster in natural categories, with the animate-inanimate distinction explaining most variance and faces forming a very focused subcluster. Human-fMRI early visual response patterns and several low-level representations of the images (luminance pattern, color pattern, silhouette pattern, V1 model representation) exhibit no

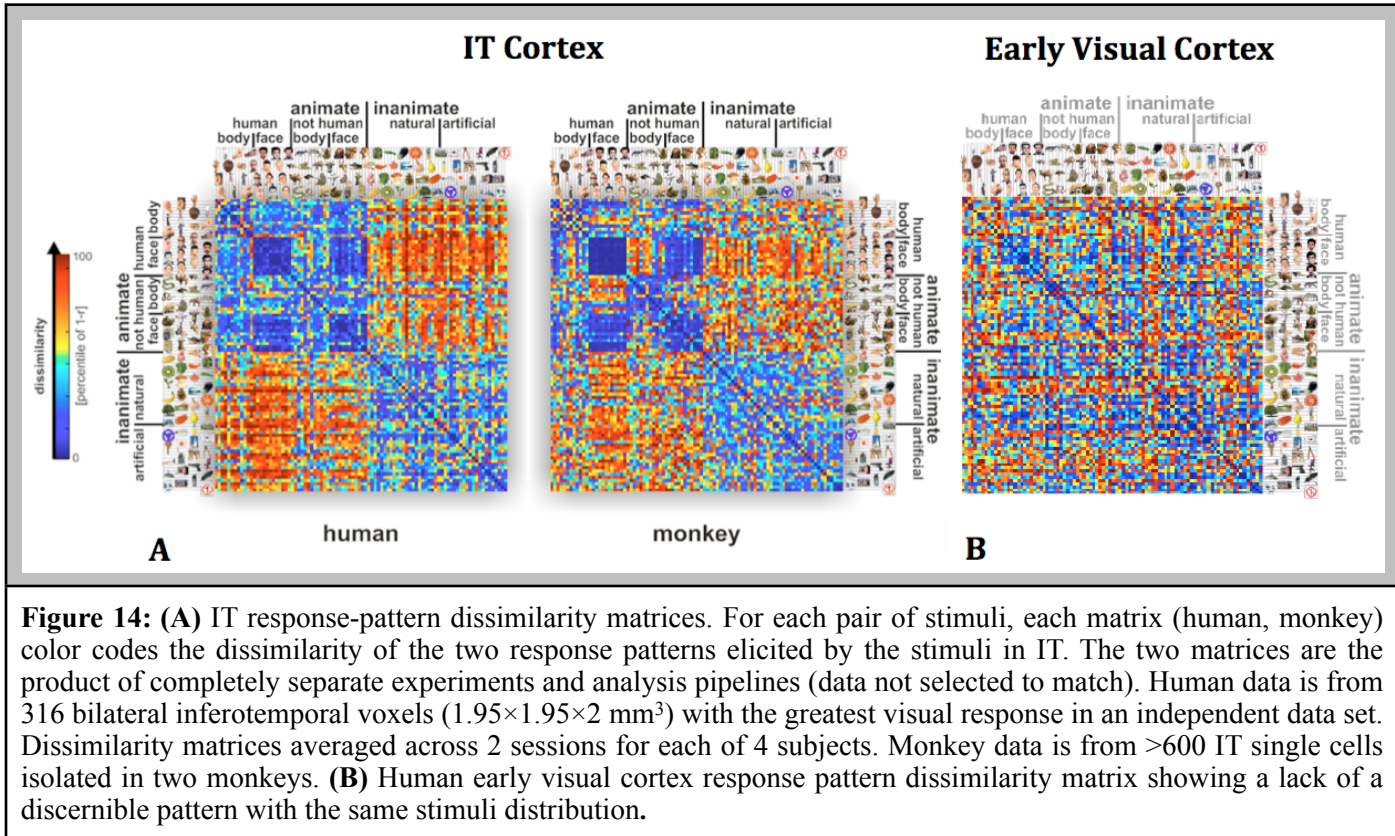


Figure 14: (A) IT response-pattern dissimilarity matrices. For each pair of stimuli, each matrix (human, monkey) color codes the dissimilarity of the two response patterns elicited by the stimuli in IT. The two matrices are the product of completely separate experiments and analysis pipelines (data not selected to match). Human data is from 316 bilateral inferotemporal voxels ($1.95 \times 1.95 \times 2 \text{ mm}^3$) with the greatest visual response in an independent data set. Dissimilarity matrices averaged across 2 sessions for each of 4 subjects. Monkey data is from >600 IT single cells isolated in two monkeys. (B) Human early visual cortex response pattern dissimilarity matrix showing a lack of a discernible pattern with the same stimuli distribution.

category clustering as shown in Figure 14B. We suspect that a computational model accounting for our results would need to have complex statistical category knowledge as might be acquired by supervised learning. Our results suggest that the extraction of information on membership in these behaviorally crucial categories constitutes a fundamental function of primate IT across species. Within the category clusters, the primate IT code appears to represent more fine-grained object information. This information as well is consistent across species and may reflect a form of visual similarity. The close match provides some hope that data from single-cell recording and fMRI, for all their differences, may consistently reveal neuronal representations when subjected to massively multivariate analyses of response-pattern information. (*J. Bodurka, H. Estekey, R. Kiani, N. Kriegeskorte, M. Mur, D. Ruff, K. Tanaka*)

2B-3. Flip angle selection for fMRI revisited

Functional MRI time series are typically dominated by nuisance or physiologic fluctuations. Flip angle choice (Ernst angle) assumes only thermal noise. In this project[2], we show that when time series are dominated by physiologic fluctuations, the flip angle choice has little impact on functional contrast to noise ratio, therefore allowing latitude in choosing a more desirable low flip angle.

In this study, we show in Figure 15, that when SNR is high and physiological noise dominates over system/thermal noise, although TSNR still reaches its maximum for the Ernst angle, reduction of imaging flip angle well below this angle results in negligible loss in TSNR. We provide a way to compute a suggested imaging flip angle, which constitutes a conservative estimate of the minimum flip angle that can be used under given experimental SNR and physiological noise levels. For our

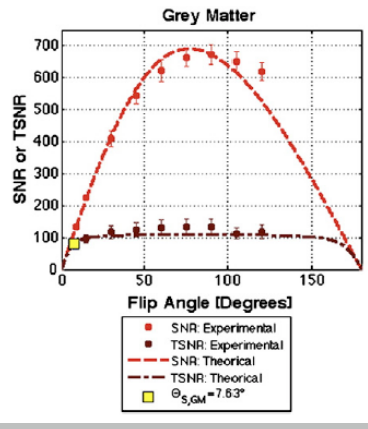


Figure 15: SNR and TSNR for GM, comparing data and simulated results. Suggested flip angle is shown as a yellow marker.

experimental conditions, this suggested angle is 7.63° for the grey matter, while the Ernst angle= 77° . Using data from eight subjects with a combined visual-motor task we show that imaging at angles as low as 9° introduces no significant differences in observed hemodynamic response time-course, contrast-to-noise ratio, voxel-

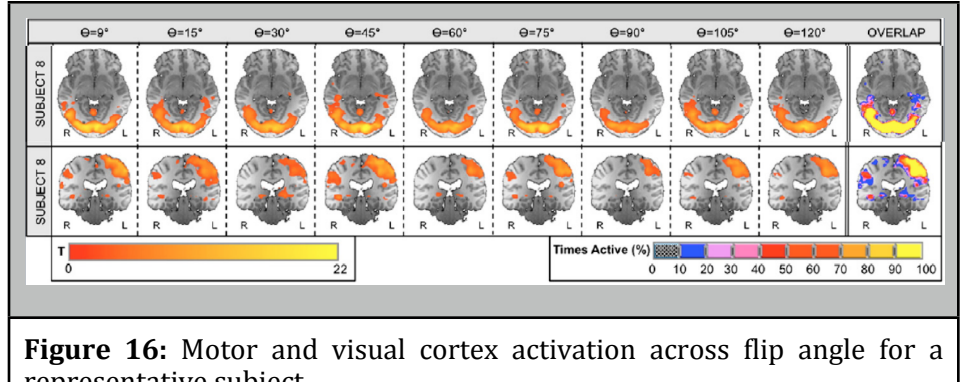


Figure 16: Motor and visual cortex activation across flip angle for a representative subject.

wise effect size or statistical maps of activation as compared to imaging at 75° (an angle close to the Ernst angle). This is shown in Figure 16. These results suggest that using low flip angles in BOLD fMRI experimentation to obtain the following benefits: reduction of RF power, reduction of apparent T1-related inflow effects, reduction of through-plane motion artifacts, lower levels of physiological noise, and improved tissue contrast is feasible when physiological noise dominates and SNR is high. (*P. A. Bandettini, N. Brenowitz, J. Gonzalez-Castillo, D. Handwerker, S. J. Inati, Z. S. Saad*)

2C. Current and Future Experiments

2C-1. Decoding of 100 ms timing differences between ocular dominance columns

We investigated the decoding of millisecond-order timing information in columnar-level neural activation from the blood oxygen level dependent (BOLD) signal in human functional magnetic resonance imaging (fMRI). In the experiment, ocular dominance columns were activated by monocular visual stimulation with 500- or 100- ms onset differences. We observed that the event-related hemodynamic response (HDR) in the human visual cortex was sensitive to the subtle onset differences, but these activation onset differences *were not reflected in hemodynamic latencies*.

We examined decoding success based on various characteristics of HDR including response amplitude, time to peak, full width at half-maximum response. This approach is shown schematically in Figure 17. We found that the timing difference was most accurately differentiated by comparison

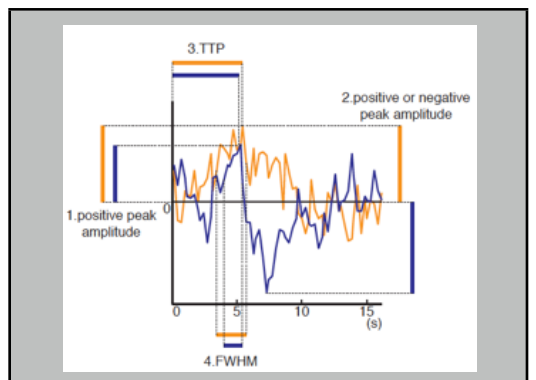


Figure 17: Responses of event-related HDR for two conditions. The explored characteristics are: 1. Positive peak amplitude 2. Pos or neg peak amplitude. 3. Time-to-peak (TTP). 4. Full-width of half maximum (FWHM).

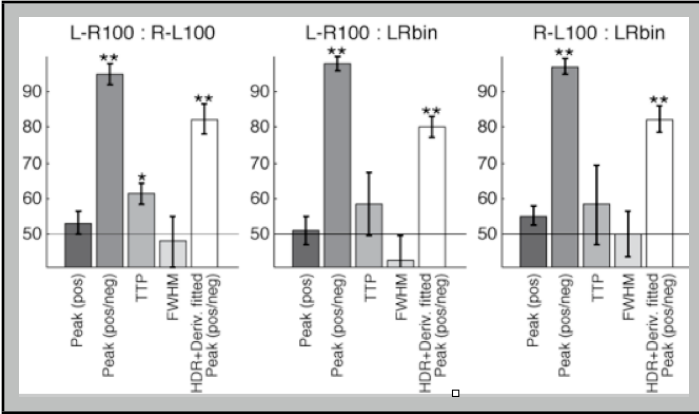


Figure 18: Decoding accuracies and their standard errors across six subjects for the extracted features of hemodynamic response shape. Asterisk (*) and double asterisk (**) indicate that the accuracy is higher than the chance level (50 %) by $p < 0.05$ and $p < 0.01$ respectively with one-sample t test.

small activations to determine how temporal delay is transferred to amplitude with regard to the BOLD response. (*P. A. Bandettini, W.-M. Luh, M. Misaki*)

2C-2. Decoding “yes” and “no.”

Towards the goal of determining the limits of sensitivity of the fMRI decoding approach, our goal was to determine if we could differentiate a simple “yes” or “no” response or subjective correctness, based on subjects’ fMRI activation patterns as they responded to simple common-knowledge questions. In each trial, we present a cue to instruct the subject to either honestly or dishonestly answer the following questions. After reading the questions, subjects have to keep their final answers in mind until a button-press prompt appears several seconds after the question are removed from the screen. At this point subjects press one of two buttons to indicate their final answers, as shown in Figure 19. 125 trials with questions about simple facts were presented in two sessions at 7T.

Based on previous research, we decided to focus on activation patterns within dorsolateral frontal cortex, in particular BA9 portion of the left middle frontal gyrus. For each trial, we extracted five time points of the voxels within this region, starting at the onset of the questions.

Treating each voxel as a feature and each time point as a sample, we trained Gaussian Naïve Bayesian (GNB) classifiers to predict the truthful Yes/No answers to the questions. A leave-two-trial-out cross-validation scheme was used to test the performance of the classifier. Specifically, in each cross-validation iteration, we left out all the samples from two trials and used the

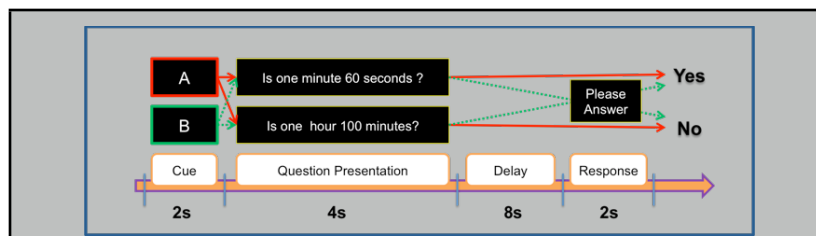


Figure 19: The experimental paradigm. At the beginning of each trial, a cue instructing the subject to answer the following question either honestly (**A**) or dishonestly (**B**). The subject was asked to generate the final answer according to his/her truthful answer and the instructed intention.

remaining samples to train the GNB classifier. The performance of the classifier was evaluated using the left-out samples. To obtain predictions for each trial (each question), we pooled the predictions for the five samples from each trial and made decisions according to their vote. The final prediction accuracy was determined by averaging the trial-wise prediction accuracies across all cross-validation iterations.

To further examine whether increasing of signal-to-noise ratio can enhance the prediction accuracy, we randomly selected trials and averaged the five samples from each trial in a point-to-point manner. GNB classifiers were trained and tested as described above. This procedure was repeated 50 times, and prediction accuracies were averaged to get the final accuracy of the classifier.

We found above-chance accuracy in trial-by-trial prediction, but also found that the prediction accuracy increased with the number of trials averaged. Figure 20 shows an accuracy curve for one subject. The mean prediction accuracy achieved 90% when we averaged all 20 trials. These findings indicate that the truthful answers are encoded in brain activity independently from intentions, and multivariate pattern analysis is able to decode them from fMRI signal. Furthermore, these results suggest that once we have sufficient signal-to-noise ratio from fMRI scans, we are able to accurately decode the truthful answers of the subjects in a single trial.
(P. A. Bandettini, Javier Gonzalez-Castillo, Z. Huang, Z. Yang)

Theme 3: Structural MRI changes, perfusion, and fMRI Calibration

3A. Introduction: Expanding the utility of fMRI and MRI

Our lab always been interested in advancing neuroimaging approaches beyond the scope of resting state or activation-based fMRI. This theme focusses on work related to this effort. Specifically, we have developed a processing pipeline for assessing anatomic changes associated with exercise and learning[4]. We also demonstrate changes in the hippocampus with an aerobic exercise intervention. With regard to perfusion imaging, we have developed in collaboration with our fMRI core facility, a high resolution, off-resonance corrected arterial spin labeling (ASL) approach at 7T, resulting in perhaps the highest quality ASL-based perfusion images yet produced[5]. In our ongoing research, we are exploring a method by which a rapid “calibration scan” can be obtained in a manner that is both easier and more accurate than either breath holding or hypercapnia for obtaining global, whole brain, signal change characteristics. We have found that the simple performance of a Valsalva maneuver can rapidly elicit signal changes that have different temporal characteristics yet similar spatial characteristics as those induced by CO₂ breathing or breath-holding. We are currently exploring the potential of this finding for implementation as a simple and repeatable global calibration stress that may be used either for assessing vascular patency or for BOLD calibration.

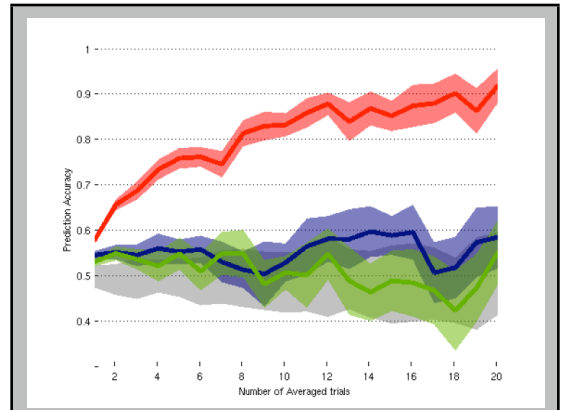


Figure 20: Prediction accuracy increases with the number of trials averaged. The red curve indicates our ROI in the overlap between Broadmann Area 9 and left middle frontal gyrus. The blue curve represents a control region in the right Insula, and the green curve represents a control region in the primary visual cortex. The color belts show the 95% confidence level. The grey belt indicates the 95% confidence interval of the null-distributions of the accuracies.

3B. Progress report

3B-1. Structural brain changes with learning and exercise

Voxel-Based Morphometry (VBM) has become a mainstay in the analysis of structural data in the neuroimaging community. It was originally used only to study differences in brain structure between different populations, but it has now become common to use this technique for determining structural changes within-subject after relatively short periods of learning. In 2009, our group was among the first to raise concerns with the way the VBM method was being used[4]. We use fMRI and three different standard implementations of longitudinal VBM: SPM2, FSL, and SPM5 to assess functional and structural changes associated with a simple learning task. Behavioral and fMRI data clearly showed a significant learning effect. However, initially positive VBM results were found to be inconsistent across minor perturbations of the analysis technique and ultimately proved to be artifactual. When alignment biases were controlled for and recommended statistical procedures were used, no significant changes in grey matter density were found. This paper demonstrated some of the potential pitfalls of existing longitudinal VBM methods and prescribes that these tools be applied and interpreted with extreme caution.

Since our 2009 paper, several other groups have echoed our concerns with longitudinal VBM. Thompson et al. [25]have uncovered severe biases in the Alzheimer's Disease Neuroimaging Initiative (ADNI). More recently Thomas and Baker [26]have published a comprehensive critique of the longitudinal VBM literature. Clearly performing accurate longitudinal analyses remains a challenge for the field. As a methodological laboratory, part of our role is to provide constructive critiques when problematic methods are employed.

There is one manipulation that the neuroimaging community agrees produces profound and lasting changes in the structure of the brain: aerobic exercise [3]. It has long been known that exercise is an effective catalyst of plasticity in animals. In collaboration with Heidi Johansen-Berg at the Oxford University, we have recently demonstrated that the hippocampus and the basal ganglia exhibit significant growth after just six weeks of aerobic exercise in a group of sedentary adults. In this study 37 sedentary participants (mean age = 31.5, 18 Males, mean VO₂Max score = 33.1 ml/kg/min) engaged in just six weeks of aerobic exercise, five days a week, 30 minutes a day (mean adherence = 28.9 sessions). Fitness assessments and MRI scans were conducted six weeks before (-6w), immediately before (0w), immediately after (+6w), and/or six weeks after

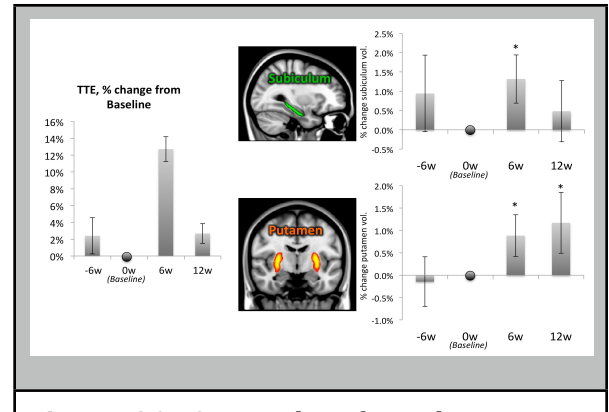


Figure 21: Six weeks of aerobic exercise training (30 minutes per day, 5 times per day) significantly increased Time To Exhaustion (TTE). After a six-week period of sedentary behavior, time to exhaustion returned to baseline levels. Increased aerobic fitness also resulted in an increased putamen volume, a region involved in motor control and learning. Putamen volume returned to baseline levels after six weeks of rest. By contrast the subiculum, a region within the hippocampus involved in memory and stress regulation, increased in volume after six weeks of aerobic exercise and the volume increase was maintained after six weeks of rest. Therefore it appears that the putamen and the subiculum have different exercise-mediated plasticities that exhibit different time courses.

the exercise period (+12w). Volumes of subcortical structures were measured in each scan session using Freesurfer and FSL tools (FIRST). Across the six-week exercise period, participants showed a mean increase in Time To Exhaustion (TTE) of 12.8% ($p<0.0001$). Figure 21 shows that there was also a significant increase in the volume of both the subiculum (a subfield of the hippocampus, 1.3%, $p<0.05$) and the putamen (part of the dorsal striatum 0.89%, $p<0.05$). Across the six-week post-exercise rest period, TTE decreased to 3% above baseline levels. Subiculum volume also returned to near baseline (with significant variance across subjects), however the volume of the putamen remained elevated. We found a significant correlation between the amount of volume change in the subiculum and the age of the participant. No such correlation was observed for the putamen, potentially suggesting a different mechanism for the structural change. Across the six-week, pre-exercise control period, no significant volume changes were observed though the subiculum showed greater variance with several subjects showing a decreased volume. This work represents the first demonstration of significant plasticity in subcortical structures after only six weeks of exercise training in sedentary adults. Additional imaging modalities will be used to explore the neural substrate of these volume changes. (P. A. Bandettini, H. Johansen-Berg, S. Marrett, A. Martin, D. A. Ruff, Z. S. Saad, A. G. Thomas)

3B-2. Robust pseudo-continuous arterial spin labeling at 7T

Pseudo-continuous arterial spin labeling (PCASL) can provide best SNR efficiency with a sufficiently long tag at high fields such as 7T, but it is very sensitive to off-resonance fields at the tagging location. We developed a robust prescan procedure to estimate the PCASL RF phase and gradient parameters required to compensate the off-resonance effects at each vessel location in about 1-2 minutes.

An incremental phase is added to each RF pulse in the labeling pulse train for both 'tag' and 'control' in a pair-wise fashion similar to traditional PCASL. This allows the pair-wise subtracted signal to follow a periodic oscillation function with zero symmetry in signal amplitude to allow for robust estimation of frequency offsets. Two thick 10mm axial slices across lateral ventricles are acquired with large voxels and 400ms post-labeling delay (PLD) to optimize SNR efficiency since intravascular tagged blood is actually beneficial to SNR. A total of 8 or 16 phases after 4 dummy volumes were acquired with 3sec TR for a scan time of 1 min and 1min 48sec, respectively. Three ROIs composed of perfusion territory for left/right carotids and vertebral arteries were selected based on pair-wise subtracted signal among sampled phases. The average signal in each ROI was fitted to a cosine function to determine the phase offset at each tagging vessel. To compensate for off-resonance fields at the tagging location, the measured offsets were applied in the subsequent PCASL scan with additional x/y gradients and fixed phase offset. After correction, all three territories have the same frequency offset. The CBF maps of 20 slices with $1.5 \times 1.5 \times 3 \text{ mm}^3$ voxels obtained in 7min after compensation are shown in Figure 24. With the proposed robust estimation and correction of frequency offsets at the tagging vessels, high quality whole-brain PCASL perfusion data of the human brain can be successfully obtained at 7T. (P. A. Bandettini, T.-Q. Li, W.-M. Luh, S. L. Talagala)

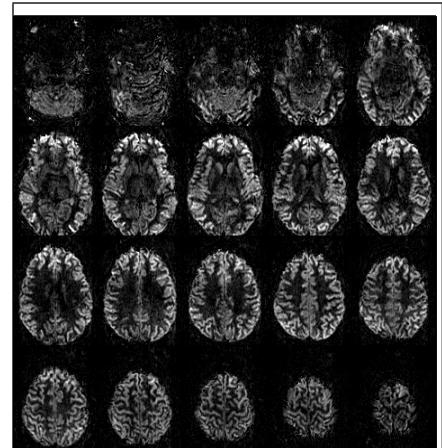


Figure 24: PCASL images obtained in 7min at 7T with $1.5 \times 1.5 \times 3 \text{ mm}^3$ resolution after compensation for off-resonance effects with x/y gradient and tagging phase offset.

3C. Current and future experiments

3C-1. Breath-holding and pressure modulation effects on cerebrovascular responses.

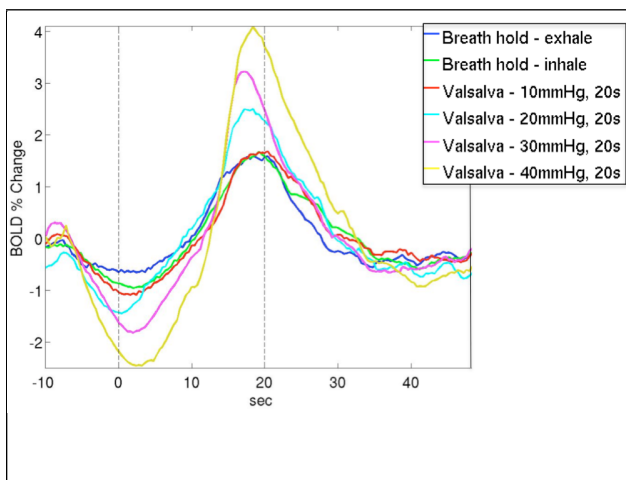


Figure 25: Curves showing gray matter response to breath hold and Valsalva demonstrating positive and negative inflections that are modulated by Valsalva pressure.

Whole-brain cerebrovascular responses are used in clinical and basic research settings. In clinical settings, information about vascular patency and susceptibility to stroke may be obtained. Cerebrovascular reactivity has also been shown to be altered in multiple sclerosis. In fMRI, a global signal change induced by breath-holding or hypercapnia induced by breathing CO₂ can be used to “calibrate” the signal - eliminating spatially variant baseline venous blood volume effects on the BOLD signal change. Calibration along with perfusion measures has also been used to obtain quantitative measures of activation-induced CMRO₂ changes.

Existing methods to cause a global cerebrovascular response are not ideal. CO₂ breathing requires a gas supply, extra hardware near the MRI scanners, and

masks over subjects' faces. Other methods use drugs, like Acetazolamide, which limit what can be done during a single scanning session since their time constants are slow. Breath-holding is convenient and can be performed by most people, but it isn't as consistent as CO₂ breathing and it's difficult to modulate cerebrovascular response magnitude, which can be used to get more accurate vascular response measures than with other methods.

We are examining a new, non-invasive way to parametrically modulate cerebrovascular response that is based on the Valsalva maneuver – an increase in chest pressure during a breath hold.

During a breath-hold we tell volunteers to blow into a non-compliant tube connected to a pressure gauge. This lets us give volunteers real-time feedback of the air pressure in their lungs. We have volunteers perform breath-holds at multiple pressure levels and with no pressure feedback. Figure 25 shows that the fMRI T2*-weighted response across cortex is modulated by chest pressure. Figure 26 shows maps that were normalized to the absolute value of the response (to compare the negative changes associated with the rapid Valsalva effect). In addition to collecting these data with T2*-weighted MRI sequence, we are collecting data using multi-echo fMRI and arterial spin label to better understand how these pressure changes alter MRI signals. (*P. A. Bandettini, D. A. Handwerker, R. M. Harper, P. Wu*)

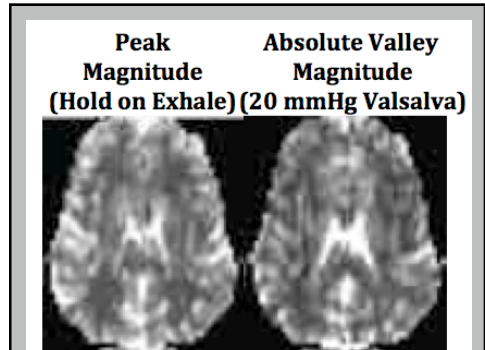


Figure 26: Comparison of fMRI signal response across breath holding and Valsalva conditions. Maps of peak positive magnitude and absolute valley magnitude appear similar across breath hold and Valsalva conditions.

References

1. Gonzalez-Castillo, J., et al., *Whole-brain, time-locked activation with simple tasks revealed using massive averaging and model-free analysis*. Proceedings of the National Academy of Sciences, 2012. **109**(14): p. 5487-5492.
2. Gonzalez-Castillo, J., et al., *Physiological noise effects on the flip angle selection in BOLD fMRI*. NeuroImage, 2011. **54**(4): p. 2764-2778.
3. Thomas, A.G., et al., *The effects of aerobic activity on brain structure*. Frontiers in psychology, 2012. **3**(86).
4. Thomas, A.G., et al., *Functional but not structural changes associated with learning: An exploration of longitudinal Voxel-Based Morphometry (VBM)*. NeuroImage, 2009. **48**(1): p. 117-125.
5. Luh, W.M., et al., *Pseudo-continuous arterial spin labeling at 7 T for human brain: Estimation and correction for off-resonance effects using a Prescan*. Magnetic Resonance in Medicine, 2012.
6. Misaki, M., et al., *Characteristic cortical thickness patterns in adolescents with autism spectrum disorders: Interactions with age and intellectual ability revealed by canonical correlation analysis*. NeuroImage, 2012. **60**(3): p. 1890-1901.
7. Mur, M., et al., *Face-identity change activation outside the face system: Release from adaptation, may not always indicate neuronal selectivity*. Cerebral Cortex, 2010. **20**(9): p. 2027-2042.
8. Mur, M., et al., *Categorical, yet graded-single-image activation profiles of human category-selective cortical regions*. Journal of Neuroscience, 2012. **32**(25): p. 8649-8662.
9. Kaplan, R., et al., *Movement-related theta rhythm in humans: Coordinating self-directed hippocampal learning*. PLoS Biology, 2012. **10**(2).
10. Knight, D.C., et al., *Learning-related diminution of unconditioned SCR and fMRI signal responses*. NeuroImage, 2010. **49**(1): p. 843-848.
11. Knight, D.C., N.S. Waters, and P.A. Bandettini, *Neural substrates of explicit and implicit fear memory*. NeuroImage, 2009. **45**(1): p. 208-214.
12. Birn, R., et al., *fMRI in the presence of task-correlated breathing changes*. NeuroImage, 2009. **47**: p. S56-S56.
13. Jones, T.B., et al., *Sources of group differences in functional connectivity: an investigation applied to autism spectrum disorder*. NeuroImage, 2010. **49**(1): p. 401-414.
14. Birn, R.M., et al., *Neural systems supporting lexical search guided by letter and semantic category cues: A self-paced overt response fMRI study of verbal fluency*. NeuroImage, 2010. **49**(1): p. 1099-1107.

15. Ruff, D.A., et al., *Complementary Roles of Systems Representing Sensory Evidence and Systems Detecting Task Difficulty During Perceptual Decision Making*. Frontiers in Neuroscience, 2010. **4**.
16. Murphy, K., et al., *The impact of global signal regression on resting state correlations: Are anti-correlated networks introduced?* Neuroimage, 2009. **44**(3): p. 893-905.
17. Kundu, P., et al., *Differentiating BOLD and non-BOLD signals in fMRI time series using multi-echo EPI*. NeuroImage, 2012. **60**(3): p. 1759-1770.
18. Handwerker, D., et al., *Periodic changes in fMRI connectivity*. NeuroImage, 2012. **in press**.
19. Fox, M.D., et al., *The human brain is intrinsically organized into dynamic, anticorrelated functional networks*. Proceedings of the National Academy of Sciences of the United States of America, 2005. **102**(27): p. 9673-9678.
20. Power, J.D., et al., *Spurious but systematic correlations in functional connectivity MRI networks arise from subject motion*. NeuroImage, 2012. **59**(3): p. 2142-2154.
21. Killackey, H.P., et al., *The relation of corpus callosum connections to architechtonic fields and body surface maps in sensorimotor cortex of new and old world monkeys*. The Journal of Comparative Neurology, 1983. **219**: p. 384-419.
22. Kiani, R., et al., *Object category structure in response patterns of neuronal population in monkey inferior temporal cortex*. Journal of Neurophysiology, 2007. **97**(6): p. 4296-4309.
23. Kriegeskorte, N., et al., *Matching Categorical Object Representations in Inferior Temporal Cortex of Man and Monkey*. Neuron, 2008. **60**(6): p. 1126-1141.
24. Kriegeskorte, N., R. Cusack, and P. Bandettini, *How does an fMRI voxel sample the neuronal activity pattern: Compact-kernel or complex spatiotemporal filter?* NeuroImage, 2010. **49**(3): p. 1965-1976.
25. Thompson, W.K. and D. Holland, *Bias in tensor based morphometry stat-ROI measures may result in unrealistic power estimates*. NeuroImage, 2011. **57**: p. 1-4.
26. Thomas, C. and C.I. Baker, *Teaching an adult brain new tricks: a critical review of evidence for training-dependent structural plasticity in humans*. NeuroImage, 2012. **in press**.

List of SFIM publications since last BSC report (papers featured in BSC report are in red)

- 1) R. M. Birn, M. A. Smith, T. B. Jones, P. A. Bandettini, The respiration response function: the temporal dynamics of fMRI signal fluctuations related to changes in respiration. *NeuroImage*, **40**, 644-654 (2008)
- 2) J. E. Dunsmoor, P. A. Bandettini, D. A. Knight, Neural correlates of unconditioned response diminution during Pavlovian conditioning. *NeuroImage* **40**, 811-817 (2008)
- 3) A. Tuan, R. M. Birn, P. A. Bandettini, G. M. Boynton, Differential transient MEG and fMRI responses to visual stimulation onset rate. *International Journal of Imaging Systems and Technology* **18**, 17-28 (2008)
- 4) R. M. Birn, K. Murphy, P. A. Bandettini, The effect of respiration variations on independent component analysis of resting state functional connectivity. *Human Brain Mapping* **29**, 740-750 (2008)
- 5) P. A. Bandettini, E. Bullmore, Endogenous oscillations and networks in functional MRI, *Human Brain Mapping* **29**, 737-739 (2008)
- 6) N. Kriegeskorte, NJ. Bodurka, and P. Bandettini, Artifactual time course correlations in echo-planar fMRI with implications for studies of brain function. *International Journal of Imaging Systems and Technology*, **18** (5-6), 345-349 (2008)
- 7) N. Kriegeskorte, M. Mur, D. Ruff, R. Kiani, J. Bodurka, H. Esteky, K. Tanaka, P. Bandettini, Matching categorical object representations in inferotemporal cortex of man and monkey. *Neuron* **60**, 1-16 (2008) (2B-2)
- 8) T. B. Jones, P. A. Bandettini, R. M. Birn, Integration of motion correction and physiological noise regression in fMRI, *NeuroImage* **42**, 582-590 (2008)
- 9) K. Murphy, R. M. Birn, D. A. Handwerker, T. B. Jones, P. A. Bandettini, The impact of global signal regression on resting state correlations: are anti-correlated networks introduced? *NeuroImage* **44**, 893-905 (2008) (1B-1)
- 10) J. Illes, M. P. Kirsch, E. Edwards, P. Bandettini, M.K. Cho, P. J. Ford, G. H. Glover, J. Kulynych, R. Macklin, D. B. Michael, S. M. Wolf, T. Grabowski, B. Seto, Practical approaches to incidental findings in brain imaging research, *Neurology*, **70**, 384-390 (2008).
- 11) J. D. Van Horn, P. A. Bandettini, K. Cheng, G. F. Egan, A. Stenger, S. Strother, A. W. Toga, New horizons for the next era of human brain imaging, cognitive, and behavioral research: pacific rim interactivity. *Brain Imaging and Behavior* **2**, 227-231 (2008).
- 12) N. Kriegeskorte, M. Mur, P.A. Bandettini, Representational similarity analysis - connecting the branches of systems neuroscience. *Frontiers in Systems Neuroscience*. doi:10.3389/neuro.06.004.2008 (2008)

- 13) P. A. Bandettini, What's New in Neuroimaging Methods?, *Annals of the NY Academy of Sciences: The Year in Cognitive Neuroscience* 2009, 260-293 (2009)
- 14) P. T. Fox, E. Bullmore, P. A. Bandettini, J. L. Lancaster, Protecting peer-review: correspondence chronology and ethical analysis regarding Logothetis vs. Shmuel and Leopold, *Human Brain Mapping*.30, 347-354 (2009)
- 15) M. Mur, P. A. Bandettini, N. Kriegeskorte, Revealing representational content with pattern-information fMRI – an introductory guide. *Social, Cognitive, and Affective Neuroscience* 4, 101-109 (2009).
- 16) D. C. Knight, J. S. Waters, P. A. Bandettini, Neural substrates of explicit and implicit fear memory, *NeuroImage*, 45, 208-214 (2009)
- 17) A. G. Thomas, S. Marrett, Z. S. Saad, D. A. Ruff, A. Martin, P. A. Bandettini, Functional but not structural changes associate with learning: an exploration of longitudinal voxel based morphometry (VBM). *NeuroImage* 48, 117-125 (2009) (3B-1)
- 18) R. M. Birn, K. Murphy, D. A. Handwerker, P. A. Bandettini, fMRI in the presence of task-correlated breathing variations, *NeuroImage* 47, 1092-1104 (2009)
- 19) P. T. Fox, E. Bullmore, P. A. Bandettini, J. L. Lancaster, Editorial reply to Jackle, *Human Brain Mapping*, 30: 1936-1937 (2009)
- 20) P. A. Bandettini, Seven Topics in Functional Magnetic Resonance Imaging. *Journal of Integrative Neuroscience*, J. Integr. Neurosci, 8 (3) 371 – 403 (2009)
- 21) D. A. Handwerker and P. A. Bandettini, Hemodynamic signals not predicted? Not so: A comment on Sirotin and Das (2009). Followup: *NeuroImage* 55, 4:1409-1412 (2011)
- 22) D. C. Knight, N. S. Waters, M. K. King, P. A. Bandettini, Learning related diminution of unconditioned SCR and fMRI signal responses. *NeuroImage* 49, 843-848 (2010)
- 23) T. B. Jones, P. A. Bandettini, L. Kenworthy, L. K. Case, S. C. Milleville, A. Martin, R. Birn, Sources of group differences in functional connectivity: an investigation applied to autism spectrum disorder. *NeuroImage* 49 (1) 401-414 (2010)
- 24) R. M. Birn, L. Kenworthy, L. Case, R. Caravella, T. B. Jones, P. A. Bandettini, A. Martin, Neural systems supporting lexical search guided by letter and semantic category cues: a self-paced overt response fMRI study of verbal fluency. *NeuroImage* 49 (1) 1099-1047 (2010)
- 25) M. Mur, D. A. Ruff, J. Bodurka, P. A. Bandettini, N. Kriegeskorte, Face-identity change activation outside the face system: “release from adaptation” may not always indicate neuronal selectivity. *Cerebral Cortex* (2010)
- 26) N. Kriegeskorte, R. Cusack, P. Bandettini, How does an fMRI voxel sample the neuronal activity pattern: compact-kernal or complex spatiotemporal filter? *NeuroImage*, 49, 1965-1976 (2010). (2C-1)

- 27) M. Misaki, Y. Kim, P. A. Bandettini, N. Kriegeskorte, Comparison of multivariate classifiers and response normalizations for pattern-information fMRI. *NeuroImage*, 53, 103-118, (2010)
- 28) D. A. Ruff, S. Marrett, H. R. Heekeren, P. A. Bandettini, L. G. Ungerleider, Complementary roles of systems representing sensory evidence and systems detecting task difficulty during perceptual decision making. *Front. Neurosci.* 4:190. Doi:10.3389/fnins.2010.00190. (2010) [\[CrossRef\]](#)
- 29) D. A. Handwerker and P. A. Bandettini, Simple explanations before complex theories: Alternative interpretations of Sirotin and Das' observations. *NeuroImage* 55, 4:1419-1422 (2011)
- 30) J. Gonzalez-Castillo, V. Roopchansingh, P. A. Bandettini, J. Bodurka, Physiological noise effects on the flip angle selection in BOLD fMRI. *NeuroImage* 54 (4) pp. 2764 – 2778. (2011) (2B-3)
- 31) P. A. Bandettini, R. Bowtell, P. Jezzard, R. Turner, Ultra-high field systems and applications at 7T and beyond: progress, pitfalls, and potential. *Magnetic Resonance in Medicine* 67, pp. 317-321 (2012)
- 32) S. M. Smith, P. A. Bandettini, K. L. Miller, T. E. J. Behrens, K. J. Friston, O. David, T. Liu, M. W. Woolrich, T. E. Nichols, The danger of systematic bias in group-level fMRI-lag-based causality estimation. *NeuroImage* 59, pp. 1228-1229 (2012)
- 33) J. Gonzalez-Castillo, Z. Saad, D. A. Handwerker, P. A. Bandettini, Whole-brain, time-locked activation with simple tasks revealed using massive averaging and model-free analysis. *Proceedings of the National Academy of Sciences* 109, 14: pp. 5487-5492 (2012) (2B-1)
- 34) C. Chu, A.-L. Hsu, K.-H. Chou, P. Bandettini, C.-P. Lin, Does feature selection improve classification accuracy? Impact of sample size and feature selection on classification using anatomical magnetic resonance images. *NeuroImage* 60, pp. 59-70 (2012)
- 35) D. A. Handwerker, V. Roopchansingh, P. A. Bandettini, Periodic changes in brain connectivity, *NeuroImage* (in press) (2012) (1B-3)
- 36) P. A. Bandettini, E. C. Wong, Sewer pipe, wire, epoxy, and finger tapping: the start of fMRI at the Medical College of Wisconsin. *NeuroImage* 62, pp. 620-631 (2012). [\[CrossRef\]](#)
- 37) P. Kundu, S. J. Inati, J. W. Evans, W.-M. Luh, P. A. Bandettini, Differentiating BOLD and non-BOLD signals in fMRI time series using multi-echo EPI. *NeuroImage* 60, pp. 1759-1770 (2012) (1B-2)
- 38) P. A. Bandettini, Functional MRI: a confluence of fortunate circumstances. *NeuroImage* 61, pp. A3-A11 (2012). [\[CrossRef\]](#)
- 39) M. Misaki, G. L. Wallace, N. Dankner, A. Martin, P. A. Bandettini, Characteristic cortical thickness patterns in adolescents with autism spectrum disorders: Interactions with age and intellectual ability revealed by canonical correlation analysis. *NeuroImage* 60, pp. 1890-1901 (2012)

- 40) D. A. Handwerker, J. Gonzalez-Castillo, M. D'Esposito, P. A. Bandettini, The continuing challenge of understanding and modeling hemodynamic variation in fMRI. *NeuroImage* 62, pp. 620-631 (2012).
- 41) J. Gonzalez-Castillo, K. N. Duthie, Z. S. Saad, C. Chu, P. A. Bandettini, W.-M. Luh, Effects of image contrast on functional MRI image registration. *NeuroImage* (in press).
- 42) P. A. Bandettini, Twenty years of Functional MRI: The Science and the Stories. *NeuroImage* 62, pp. 575-588 (2012). [\[CrossRef\]](#)
- 43) W.-M. Luh, S. L. Talagala, T.-Q. Li, P. A. Bandettini, Pseudo-continuous arterial spin labeling at 7T for human brain: estimation and correction for off-resonance effects using a prescan, *Magn. Reson. Med.* (in press) (3B-2)
- 44) M. Mur, D. A. Ruff, J. Bodurka, P. De Weerd, P. A. Bandettini, N. Kriegeskorte, Categorical, yet graded single-image activation profiles in human category-selective cortical regions, *The Journal of Neuroscience*, 32, pp. 8649-8662 (2012)
- 45) Z. Yang, X.-N Zuo, P. Wang, Z. Li, S. M. LaConte, P. A. Bandettini, X. P. Hu, Generalized RAICAR: Discover homogeneous subject (sub)groups by reproducibility of their intrinsic connectivity networks, *NeuroImage* (in press).
- 46) R. Kaplan, C. F. Doeller, G. R. Barnes, V. Litvak, E. Duzel, P. A. Bandettini, N. Burgess, Movement-related theta rhythm in humans: coordinating self-directed hippocampal learning. *PloS Biology*, 10, e1001267 (2012)
- 47) A. G. Thomas, A. Dennis, P. A. Bandettini, H. Johansen-Berg, The effects of aerobic activity on brain structure. *Frontiers in Psychology*, 3, 1-9 (2012) (3B-1)

Section 3: Resources Requested

Currently, SFIM personnel consists of the following personnel:

Chief, Peter Bandettini
Research Fellow, Javier Gonzalez-Castillo
Research Fellow, Daniel Handwerker
Research Fellow, Hang Joon Jo (starting in Jan)
Research Fellow, (currently open and being filled)
Predoc IRTA (GPP), Prantik Kundu
Predoc IRTA (GPP), Raphael Kaplan
Postbac IRTA, Paula Wu
Postbac IRTA, Colin Hoy
IT Desktop Specialist, Joseph Naegele
IT Specialist, (currently open and being filled)
Staff Scientist (open, yet do not have funding to fill this)
Special Volunteer (post-doc), Jennifer Evans
Special Volunteer (post-doc), Zhi Yang

I would like to request the following:

1. Two more Postbac IRTA positions and funding to pay for them.
2. Funding to fill my open title 42 staff scientist position.

Justification for request #1. A formula that has worked well for my group in the past is to have one post bac IRTA for each post doc or research fellow. This works extremely well in that each research fellow then supervises a post bac IRTA, thus gaining supervisory experience and providing one-on-one time with the post bac IRTA who then, after one year, works on a small project of their own. I have four post docs and only two post bac IRTAs. I'm therefore requesting two more post bac IRTAs.

Justification for request #2. In 2009, my Staff Scientist, Rasmus Birn left to obtain an assistant professor position at University of Wisconsin, Madison. I was in the process of filling his position when he informed me that he was considering coming back. I left the position open as I expected him to return. After about a year of planning to return, he decided, in the end, to stay in Madison. In the mean time, because I took too long to fill the position, I was no longer credited with having the position when we had our budget cuts. I was left with an open staff scientist position but no funds to pay for it. Other tenured PIs who have been at the NIH for over 13 years with all Outstanding ratings for their past BSC reviews I imagine have at least one and more likely two staff scientists. I currently have none. Although we are maintaining a high level of productivity without one, I am concerned that the scientific continuity of the section will be lost once my senior post docs move on.

As a final note, after my last BSC review in 2007, which I had received "Outstanding," I was told by the scientific director that none of my requests would be fulfilled. If my scores merit it this time, I hope that the NIMH budget is such that these relatively small requests could be fulfilled.